Published in the proceedings of the 20th IAHR Symposium,
August 6-9 2000, Charlotte, North Carolina, U.S.A. http://www.hcipub.com/iahr2000

A Numerical Comparison of Four Operating Conditions in a Kaplan Water Turbine, Focusing on Tip Clearance Flow

H. Nilsson[1] and L. Davidson[2]

ABSTRACT

A parallel multiblock finite volume CFD (Computational Fluid Dynamics) code CALC-PMB [3, 10, 11] (Parallel MultiBlock) for computations of turbulent flow in complex domains has been developed and used for the computations of the flow through a Kaplan water turbine. The computations are including both the guide vanes and the runner, where the runner computations get the inlet boundary conditions from the circumferentially averaged properties of the guide vane computations. Four different operating conditions have been computed and the results from the computations are compared. The computational results are in accordance with observations done by the the turbine manufacturer. This work is focused on tip clearance flow, which reduces the efficiency of the turbine by about 0.5%.

INTRODUCTION

This work is focused on tip clearance losses in Kaplan water turbines, which reduces the efficiency of the turbine by about 0.5%. This work is part of a Swedish water turbine program financed by a collaboration between the Swedish power industry via ELFORSK (Swedish Electrical Utilities Research and Development Company), the Swedish National Energy Administration and GE Energy (Sweden) AB. The purpose of the Swedish water turbine program is to increase Swedish water power competence in order to meet the growing water power demand in Sweden and demands on preservation of the environment and efficiency.

The main features of the CALC-PMB CFD code are the use of conformal block structured boundary fitted coordinates, a pressure correction scheme (SIMPLEC [4]), cartesian velocity components as the principal unknowns, and collocated grid arrangement together with Rhie and Chow interpolation. The discretization schemes used in this work are a second-order Van Leer scheme for convection and a second order central scheme for the other terms. The computational blocks are solved in parallel with Dirichlet-Dirichlet coupling using PVM (Parallel Virtual Machine) or MPI (Message Passing Interface). The parallel efficiency is excellent, with super scalar speedup for load balanced applications [1, 10]. The ICEM CFD/CAE grid generator is used for grid generation and Ensight and Matlab are used for post-processing.

The investigated turbine is a test rig with a runner diameter of $0.5m$. It has four runner blades and 24 guide vanes. The tip clearance between the runner blades and the shroud is $0.25mm$. To resolve the turbulent flow in the tip clearance and the boundary layers, a low Reynolds number turbulence model is used. Because of computational restrictions, complete turbine simulations found in the literature usually use wall functions instead of resolving the boundary layers, which makes tip clearance investigations impossible. Since part of the computational domain is rotating, Coriolis and centripetal effects are included in the momentum equations. At this stage, the $k-\omega$ model of Wilcox [13], which can be integrated all the way to the wall, is used without terms for rotational effects. This is common in turbomachinery computations for reasons of numerical stability and the small impact of such terms in these kinds of industrial

[1]Tech.Lic., CHALMERS, Thermo and Fluid Dynamics, S - 412 96 Gothenburg, Sweden, hani@tfd.chalmers.se
[2]Professor, CHALMERS, Thermo and Fluid Dynamics, S - 412 96 Gothenburg, Sweden, lada@tfd.chalmers.se

applications. To resolve the turbulent boundary layers and the tip clearance at the same time that the grid size should be kept as low as possible and the control volumes as orthogonal as possible, the computational grid is created in a multiblock topology using ICEM CFD/CAE. During the computations, the computational blocks are assigned to separate PVM or MPI processes. The level of parallelization is thus determined by the block size distribution and the distribution of the processes on the available processors.

Since the computations involve both rotating and stationary frames of references, the interaction between these is numerically very complicated. A simple approach is used in this work where the computations are performed in two steps. The stationary guide vanes are first computed without any interaction from the runner blades. The rotating runner is then computed, using the circumferentially averaged velocities and turbulent quantities from the guide vane computations at the trailing edge of the guide vanes. The upstream effect from the runner blades on the flow at the guide vanes is neglected. The computations of both the guide vanes and the runner are confined to a single guide vane or runner blade. This includes no extra restrictions since the boundary conditions are assumed to be stationary axisymmetric and the stationary Reynolds averaged solution is thus periodic.

The present work investigates the flow structures of stationary periodic turbulent mean flow for different guide vane angles. The runner blade angle is kept at a constant value so that the same runner grid may be used for all cases.

EQUATIONS

The equations used for the computations are briefly described below.

The stationary Reynolds time-averaged continuity and Navier Stokes equations for incompressible flow in a rotating frame of reference read [2, 6]

$$\frac{\partial \rho U_i}{\partial x_i} = 0$$

$$\frac{\partial \rho U_i U_j}{\partial x_j} = -\frac{\partial P}{\partial x_i} + \frac{\partial}{\partial x_j}\left((\mu + \mu_t)\frac{\partial U_i}{\partial x_j}\right) + \rho g_i - \rho \epsilon_{ijk}\epsilon_{klm}\Omega_j\Omega_l x_m - 2\rho\epsilon_{ijk}\Omega_j U_k$$

where $-\epsilon_{ijk}\epsilon_{klm}\Omega_j\Omega_l x_m$ is the centripetal term and $-2\epsilon_{ijk}\Omega_j U_k$ is the Coriolis term, owing to the rotating coordinate system. Because of the potential nature of the pressure, gravitational and centripetal terms [6], they are put together during the computations, in what is often referred to as a *reduced* pressure gradient

$$-\frac{\partial P^*}{\partial x_i} = -\frac{\partial P}{\partial x_i} + \rho g_i - \rho \epsilon_{ijk}\epsilon_{klm}\Omega_j\Omega_l x_m$$

Thus, a relation for the *reduced* pressure is

$$P^* = P - \rho g_i x_i + \rho \epsilon_{ijk}\epsilon_{klm}\Omega_j\Omega_l x_m x_i$$

When post-processing, the variation of the gravity term is assumed to be negligible and the centripetal term is simply subtracted from the *reduced* pressure.

The $k-\omega$ model of Wilcox [13] for the turbulent kinetic energy, k, and the specific dissipation rate, ω, reads

$$\begin{aligned}
\frac{\partial \rho U_j k}{\partial x_j} &= \frac{\partial}{\partial x_j}\left[\left(\mu + \frac{\mu_t}{\sigma_k}\right)\frac{\partial k}{\partial x_j}\right] + P_k - \rho\beta^\star\omega k \\
\frac{\partial \rho U_j \omega}{\partial x_j} &= \frac{\partial}{\partial x_j}\left[\left(\mu + \frac{\mu_t}{\sigma_\omega}\right)\frac{\partial \omega}{\partial x_j}\right] + \frac{\omega}{k}\left(c_{\omega 1}P_k - c_{\omega 2}\rho k\omega\right)
\end{aligned}$$

Case	N_{11} $\left(\frac{ND}{\sqrt{H}}\right)$	Q_{11} $\left(\frac{Q}{D^2\sqrt{H}}\right)$	γ (guide vane angle)	η (efficiency)
k15	160.1	1.195	35.1	92.40
k138	150.0	1.136	33.3	92.62
k150	145.0	1.115	33.0	92.56
k123	140.0	1.084	31.9	92.26

Table 1: The operating conditions used in this work.

where the turbulent viscosity, μ_t, is defined as

$$\mu_t = \rho \frac{k}{\omega}$$

The production term reads

$$P_k = \mu_t \left(\frac{\partial U_i}{\partial x_j} + \frac{\partial U_j}{\partial x_i} \right) \frac{\partial U_i}{\partial x_j}$$

and the closure coefficients are defined from experiments as

$$\beta^\star = 0.09,\ c_{\omega 1} = \tfrac{5}{9},\ c_{\omega 2} = \tfrac{3}{40},\ \sigma_k = 2 \text{ and } \sigma_\omega = 2$$

At the walls a no-slip condition is applied for the velocities, $k = 0$ and at the first node normal to the wall, at $y^+ < 2.5$, $\omega = 6\nu/(C_{\omega 2} n^2)$ where n denotes the normal distance to the wall. For the pressure, the implicit inhomogeneous Neumann boundary condition $\partial^2 P/\partial n^2 = 0$ is used at all boundaries.

OPERATING CONDITIONS

The operating conditions used as test cases in this work are given in table 1, where N_{11} is the unit speed, Q_{11} is the unit flow, N is the rotational speed, Q is the volume flow, D is the runner diameter, H is the head, γ is the guide vane angle and η is the turbine efficiency. The test case names are used in presenting the results. The reason for choosing these operating conditions is that the best way to increase the blade tip load is to decrease the unit speed. An increased blade tip load leads to increased tip clearance flow and tip vortex cavitation [8]. The unit speed of the operating conditions in table 1 decreases from case k15 to case k123. Even though the efficiency is not greatest for case k15, it is decided to be the best point of operation. The reason for this is that other flow features, such as tip clearance vortex cavitation, become important for the other cases.

GUIDE VANE COMPUTATIONS

For the guide vane computations, one computational grid has been created for each operating condition. The grids are equally sized (120,344 control volumes) with similar multiblock topology to reduce grid point distribution dependencies. In figure 1(a), the computational grid for case k15 is shown as a surface grid, duplicated to four guide vanes. At the inlet, the flow is

aligned with the guide vanes and fully developed turbulent 1/7 profiles are assumed [3, 10]. The inlet turbulent kinetic energy is estimated by

$$k_{in} = C_{\mu}^{-0.5} l_m^2 \left(\frac{\partial U}{\partial y} \right)^2$$

where l_m is the Prandtl's mixing length and is given by

$$l_m = \min(\kappa y, \lambda \delta)$$

where $\kappa = 0.41$ is the von Karman constant, $\lambda = 0.09$, y is the distance from the wall and δ is the inlet height. This relation stem from the assumption of turbulence-energy equilibrium, i.e. production of turbulent kinetic energy is balanced by its dissipation. The inlet specific dissipation is set according to

$$\omega_{in} = \frac{\rho k_{in}}{10 \mu}$$

The computational domain includes the runner section but no effects of the runner are included. At the outlet fully developed Neumann boundary conditions are used. The computations are performed for a single guide vane using axisymmetric inlet boundary conditions and assuming stationary periodic flow. The purpose of the guide vane computations is to generate inlet boundary conditions for the runner computations.

RUNNER COMPUTATIONS

For the operating conditions described above, the runner blade angle is kept constant so that the same grid may be used in all cases. This saves a great deal of work and allows the results to be compared without grid dependence. The grid consists of 324,360 control volumes of which the tip clearance is resolved by 7,392 control volumes where 24 control volumes are in the runner blade tip to shroud direction. The grid is shown in figure 1(b), as a surface grid, duplicated to four runner blades. The quality of the computational results relies a great deal on the quality of the grid. Using a complicated O-grid topology like this, the control volumes can be made sufficiently orthogonal and the resolution of the boundary layers does not unnecessarily resolve other regions. The computational domain starts at the trailing edge of the guide vanes, where axisymmetric inlet boundary conditions from the guide vane computations are applied. Fully developed Neumann boundary conditions are used at the outlet, at the end of the axisymmetric diffusor before the draft tube bend. Since the computations are performed in a rotating frame of reference, the velocity on the rotating surfaces is set to zero while the velocity on the stationary surfaces is given a counter-rotating velocity component. The computations are performed for a single runner blade assuming stationary periodic flow. The main purpose of the runner computations is to investigate tip clearance flow features and their variation with decreasing unit speed.

RESULTS

The main object of the guide vane computations in this work was to produce reasonable inlet conditions for the runner computations. The circumferentially averaged velocity coefficient profiles at the trailing edge of the guide vanes (R=0.287m, figure 2) is shown in figure 3(a). The

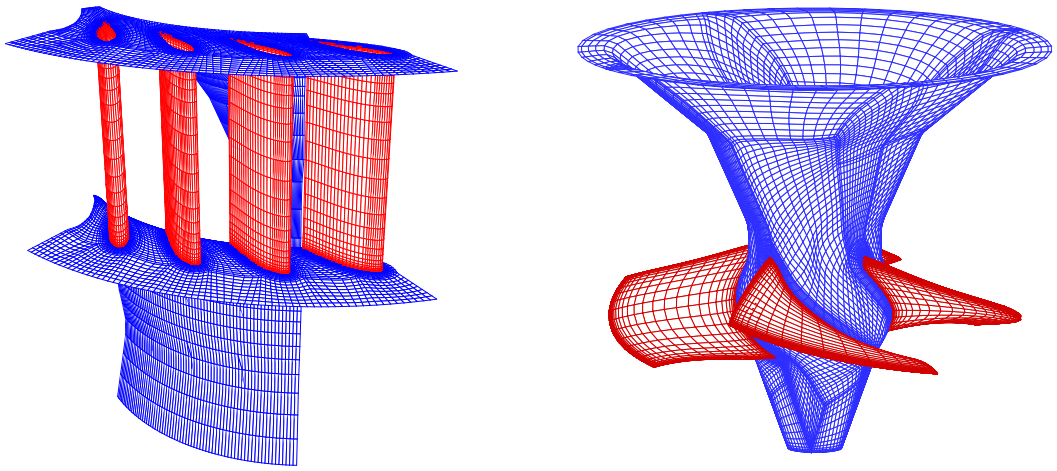

(a) Four (of 24) guide vanes for the k15 case.

(b) The Kaplan runner grid.

Figure 1: Multiblock grids of the runner and guide vanes of the Kaplan water turbine, investigated in this work. Only the grid planes attached to surfaces are shown.

distribution of the velocitiy coefficients is not uniform along the traverse line and, because of the curvature of the meridional contour of the turbine, the magnitudes of the velocity coefficients generally increase at the lower ring and decrease at the upper ring except for the radial velocity coefficient in the upper ring boundary layer. The lower ring flow has thus more dynamic and less static energy and vice versa for the upper ring flow. Among the three velocity components, the tangential velocity is the largest. The effect of deceleration in the boundary layers due to friction thus becomes largest for the tangential velocity, which is the reason why the radial velocity is accelerated in the boundary layers, corresponding to a reduction of centrifugal force [5]. These velocity coefficient profiles were used as inlet boundary conditions for the runner computations.

The general Euler equation for turbomachinery relating the input shaft power to the change in angular momentum for a thin axisymmetric stream tube can be written [7]

$$-dP_{shaft} = d\dot{m}\,\Omega\,(r_2 C_{\theta 2} - r_1 C_{\theta 1})$$

where $d\dot{m}$ is the mass flow through the stream tube, Ω is the runner rotation, r is the mean radius and C_θ is the velocity in the tangential direction in a stationary coordinate system. Index 1 denotes *before* the runner and index 2 denotes *after* the runner, which should be located far from the runner blades so that the properties can be assumed to be axisymmetric and uniform along the height of the thin stream tube. This equation is valid for a thin axisymmetric control volume where there is no mass, momentum or energy transfer through the control volume surfaces except at 1 and 2, with the exception of input shaft power transmitted to the blades in the control volume as torque. The surface forces in the tangential direction on the control volume surfaces are also assumed to be negligible. Using this relation, assuming that the stream tube surfaces follow the meridional contour of the turbine and that the mass flow distribution is similar for all the cases, the radial blade power distribution can be investigated qualitatively. Figure 3(b) shows the circumferentially averaged radial distribution of rC_θ before (y=0.071m, figure 2) and after (y=-0.137m, figure 2) the runner blades for the different cases. The main difference between these cases is that the shaft power close to the runner tip increases when the unit speed

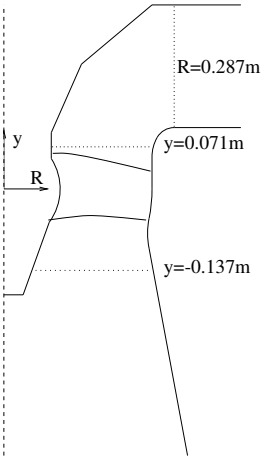

Figure 2: Circumferential averaging. The solid lines are the casing and runner blade profiles. The dashed line is the axis of rotation. The dotted lines are the positions of the circumferential averaging. The inlet boundary for the runner computations is located at R=0.287m.

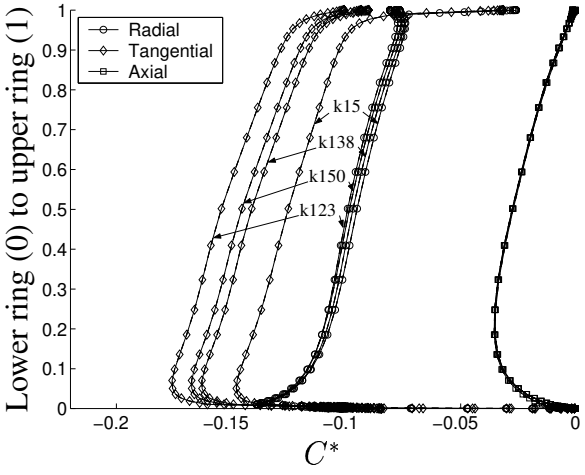

(a) The runner inlet velocities (normalized by $C_{ref} = \Omega R_{ref}$), obtained from the guide vane computations.

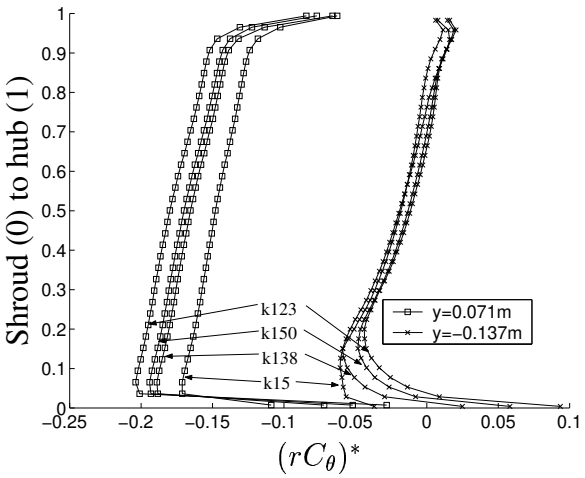

(b) The angular momentum distribution (normalized by $R_{ref}C_{ref} = R_{ref}^2\Omega$) before (y=0.071m) and after (y=-0.137m) the runner.

Figure 3: Circumferentially averaged properties of the flow. The properties are normalized using Ω, the runner rotation and R_{ref}, the turbine radius.

decreases. This is in accordance with the fact that the blade tip loading for this runner increases when the unit speed is decreased.

The pressure difference between the pressure side and the suction side of the runner blades drives a flow through the tip clearance between the runner blade tip and the shroud. It can be seen in figure 4(a) that the magnitude of the axial absolute velocity coefficient increases when the unit speed decreases. This effect is greatest close to the leading edge tip clearance, which is in accordance with both observations made by the turbine manufacturer and the inreasing blade tip loading with decreasing unit speed.

The tip clearance flow creates a jet that separates from the runner blade suction side and gives rise to a local static pressure reduction close to the tip on the suction side of the runner blade, which is the center of a tip vortex. If the static pressure in this region falls below the vapour pressure for the water flowing through the turbine, cavitation bubbles will form. Figure 4(b) shows the runner blade tip static pressure distribution in a meridional plane going through the center of a runner blade. The tip clearance jet impacts on the shroud boundary layer, where a local static pressure increment can be observed. There is also a local static pressure reduction

somewhat radially inside the tip (twice the blade tip thickness), on the suction side of the blade. A possible cavitational scenario in this case could be that a fluid particle is trapped inside the tip vortex long enough for cavitational bubbles to be formed. Escaping the tip vortex, the cavitational bubbles might follow the vortex rotation and impact on the runner blade suction side between the local static pressure minima, implode and damage the blade or they might survive into the second local static pressure minimum and be transported towards the trailing edge of the blade.

In figure 5(a), the vortex formed on the suction side of the blade, by the tip clearance jet, is visualized by a stream ribbon close to the vortex core. The stream ribbon is colored by the magnitude of the relative velocity, which shows that the magnitude of the relative velocity is reduced close to the vortex core since the velocity increases downstream where the stream ribbon escapes from the vortex core. The reduced relative velocity in combination with a low static pressure makes this region a cavitation bubble production region, since the fluid is exposed to low static pressure for longer periods of time. In the same figure, a stream ribbon emitted inside the shroud boundary layer is visualized. The shroud stream ribbon is counter-rotating, relative to the tip vortex, and it is being scraped off the shroud boundary layer by the tip clearance jet.

In figure 5(b), a static pressure 3D iso-surface visualizes where the suction side static pressure is locally reduced for the k123 case. This reveals three main regions where the static pressure is locally reduced. The first region occurs at the leading edge. In this region, the formation of sheet cavitation is often initiated. The second region occurs on the suction side of the blade surface. Close to this region, major runner blade cavitation damage is often observed. The third region occurs at the tip clearance vortex core, as described above. According to the turbine manufacturer, the studied Kaplan runner is not supposed to run at this operating condition owing to the erosional effects of cavitation.

VALIDATION

For the present investigation, the only information available is the geometry definitions and the operating conditions in table 1. The validation of the computations thus relies on validations performed for other applications [3, 9] and an ongoing project, where the code is validated against the GAMM [12] Francis turbine.

The correct solution is assumed to be reached when the largest normalized residual of the momentum equations, the continuity equation and the turbulence equations is reduced to 10^{-3} [10]. The momentum equation residuals are normalized by the sum of the mass flow through the turbine and the mass flow through the periodic surfaces multiplied by the largest value of the velocity component of each equation. The continuity equation residual is normalized by the sum of the mass flow through the turbine and the mass flow through the periodic surfaces. The turbulence equations residuals are normalized by the largest residual during the iterations.

DISCUSSION

As mentioned, the reason for choosing the operating conditions used in this work is that the best way to increase the blade tip load is to decrease the unit speed. An increased blade tip load leads to increased tip clearance flow and tip vortex cavitation. The numerical analysis performed has shown that these flow features have been captured by the computations: The blade tip loading increases when the unit speed decreases. The magnitude of the computed tip clearance velocity coefficients increases when the unit speed decreases. This is particularly

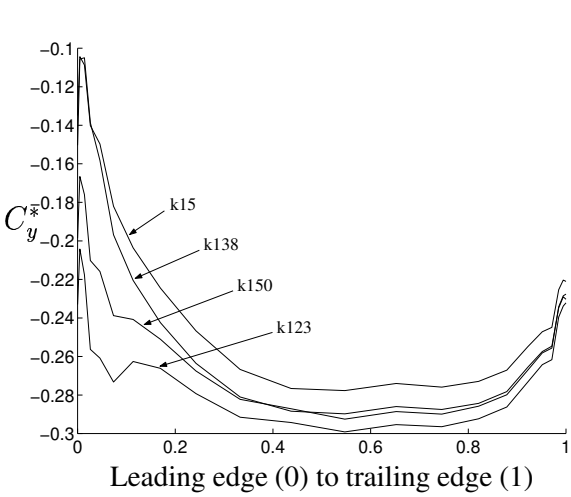

(a) The axial absolute velocity coefficients ($C_y^* = C_y/(\Omega R_{ref})$, where Ω is the runner rotation and R_{ref} is the turbine radius) of the tip clearance flow. The velocities are averaged from runner blade tip to shroud.

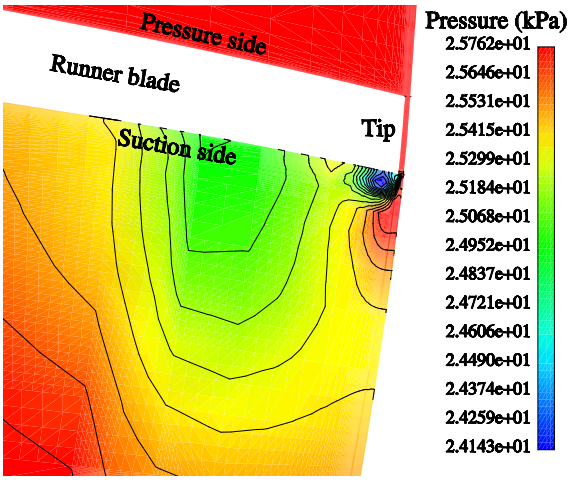

(b) The pressure distribution close to the tip clearance for case k15, visualized as a contour plot in a meridional plane going through the center of the blade. The level of the pressure is not adjusted to a real case, since it is the pressure gradients that are important in this figure.

Figure 4: Flow features at the tip clearance, between the runner blade tip and the shroud.

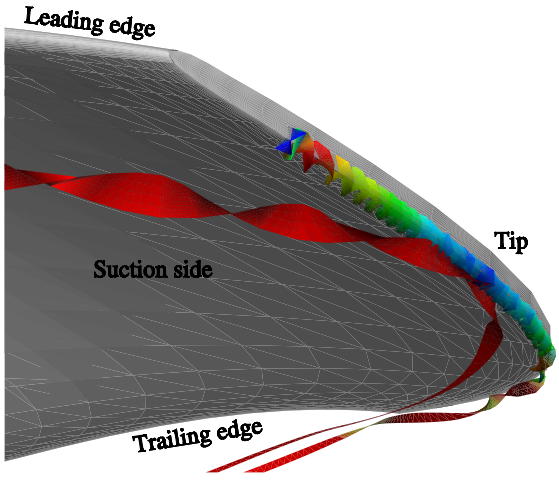

(a) Tip vortex core and shroud boundary layer stream ribbons, colored by the magnitude of the relative velocity (red is high and blue is low)

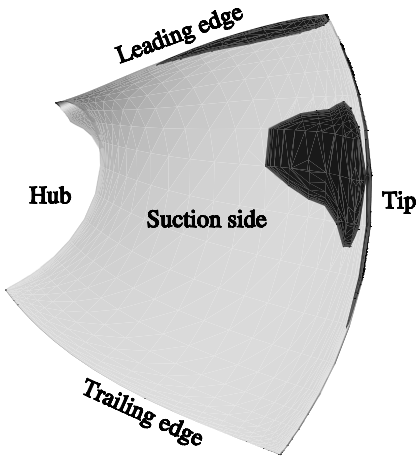

(b) A static pressure 3D iso-surface, indicating where the suction side static pressure is locally reduced (dark regions) for the k123 case.

Figure 5: Runner blade suction side effects.

significant at the leading edge of the tip clearance. The tip vortex core has a reduced static pressure and reduced relative velocities. Three main regions of suction side local static pressure reduction are observed. These flow features are in accordance with observations made by the turbine manufacturer.

In this work, the upstream effects from the runner on the guide vane flow and the transient effects of non-axisymmetric runner inlet boundary conditions are excluded. In particular, the non-axisymmetric runner inlet boundary conditions are expected to affect the dynamics of the tip vortex because of the varying angles of incidence. In the future, a more advanced coupling between the rotating and stationary parts together with transient computations will be used to include the transient effects of guide vane wakes, varying angles of incidence and the instabilities of the tip vortex.

The introduction of CFD in the area of hydraulic machine research is believed to increase a detailed knowledge of the flow inside the machines and to speed up the design procedure. This requires that the experience from CFD in this area is increased, which cannot be achieved without detailed experimental investigations to be used for comparisons. With sufficient experience of CFD in the area of hydraulic machine research, CFD will definitely be used in future hydraulic machine development.

References

[1] S. Dahlström, H. Nilsson, and L. Davidson. Lesfoil: 6-months progress report by Chalmers. Technical report, Dept. of Thermo and Fluid Dynamics, Chalmers University of Technology, Gothenburg, 1998.

[2] L. Davidson. An introduction to turbulence models. Int.rep. 97/2, Thermo and Fluid Dynamics, Chalmers University of Technology, Gothenburg, 1997.

[3] L. Davidson and B. Farhanieh. CALC-BFC: A Finite-Volume Code Employing Collocated Variable Arrangement and Cartesian Velocity Components for Computation of Fluid Flow and Heat Transfer in Complex Three-Dimensional Geometries. Rept. 92/4, Thermo and Fluid Dynamics, Chalmers University of Technology, Gothenburg, 1992.

[4] J.P. Van Doormaal and G.D. Raithby. Enhancements of the SIMPLE method for predicting incompressible fluid flows. *Num. Heat Transfer*, 7:147–163, 1984.

[5] T. Kubota. Normalization of flow profile data measured at runner inlet. In G. Sottas and I. L. Ryhming, editors, *3D-Computations of Incompressible Internal Flows - Proceedings of the GAMM Workshop at EPFL, September 1989, Lausanne - Notes on Numerical Fluid Mechanics*, pages 55–62. Vieweg, Braunschweig, 1993.

[6] P.K. Kundu. *Fluid Mechanics.* Academic Press, San Diego, California, 1990.

[7] B. Lakshminarayana. *Fluid Dynamics and Heat Transfer of Turbomachinery.* John Wiley & Sons, Inc., New York, 1996.

[8] B. Nauclér. Private communication. *Kvaerner Turbin AB*, 1998.

[9] H. Nilsson. A parallel multiblock extension to the CALC-BFC code using pvm. Int.rep. 97/11, Dept. of Thermo and Fluid Dynamics, Chalmers University of Technology, Gothenburg, 1997.

[10] H. Nilsson. A Numerical Investigation of the Turbulent Flow in a Kaplan Water Turbine Runner. Thesis for the degree of Licentiate of Engineering 99/5, Dept. of Thermo and Fluid Dynamics, Chalmers University of Technology, Gothenburg, 1999.

[11] H. Nilsson and L. Davidson. CALC-PVM: A parallel SIMPLEC multiblock solver for turbulent flow in complex domains. Int.rep. 98/12, Dept. of Thermo and Fluid Dynamics, Chalmers University of Technology, Gothenburg, 1998.

[12] G. Sottas and I. L. Ryhming, editors. *3D-Computations of Incompressible Internal Flows - Proceedings of the GAMM Workshop at EPFL, September 1989, Lausanne - Notes on Numerical Fluid Mechanics.* Vieweg, Braunschweig, 1993.

[13] D.C. Wilcox. Reassessment of the scale-determining equation for advanced turbulence models. *AIAA J.*, 26(11):1299–1310, 1988.